



This open access document is published as a preprint in the Beilstein Archives with doi: 10.3762/bxiv.2019.147.v1 and is considered to be an early communication for feedback before peer review. Before citing this document, please check if a final, peer-reviewed version has been published in the Beilstein Journal of Organic Chemistry.

This document is not formatted, has not undergone copyediting or typesetting, and may contain errors, unsubstantiated scientific claims or preliminary data.

Preprint Title Facile synthesis and assessment of 2-alkoxy-4-(4-hydroxyphenyl)-6-arylnicotinonitrile derivatives as new inhibitors for C1018-steel corrosion in HCl: A combined theoretical and experiential investigations

Authors Hany Abd El-Lateef, Antar A. Abdelhamid, Mounir A. A. Mohamed and Amr H. Moustafa

Publication Date 26 Nov 2019

Article Type Full Research Paper

Supporting Information File 1 Supplementary Material.doc; 1.3 MB

ORCID® IDs Hany Abd El-Lateef - <https://orcid.org/0000-0002-6610-393X>; Antar A. Abdelhamid - <https://orcid.org/0000-0002-2814-7499>; Amr H. Moustafa - <https://orcid.org/0000-0001-7242-6527>

Facile synthesis and assessment of 2-alkoxy-4-(4-hydroxyphenyl)-6-arylnicotinonitrile derivatives as new inhibitors for C1018-steel corrosion in HCl: A combined theoretical and experiential investigations

Hany M. Abd El-Lateef^{ra,b*1}, Antar A. Abdelhamid^{c*1}, Mounir A.A. Mohamed^d, Amr H. Moustafa^c

^a *Physical Chemistry Lab., Chemistry Department, Faculty of Science, Sohag University, 82524 Sohag, Egypt*

^b Department of Chemistry, College of Science, King Faisal University, Al-Hofuf, Al-Ahsa 31982, Saudi Arabia

^c *Synthetic Organic Chemistry Lab., Chemistry Department, Faculty of Science, Sohag University, 82524 Sohag, Egypt*

^d *Theoretical Chemistry Lab., Chemistry Department, Faculty of Science, Sohag University, 82524 Sohag, Egypt*

* Corresponding authors: hmahmed@kfu.edu.sa, Hany_shubra@yahoo.co.uk (Hany M. Abd El-Lateef); drantar25@yahoo.com (Antar A. Abdelhamid)

Abstract

An effective and accessible synthesis of alkoxy arylnicotinonitriles was achieved *via* a four-component reaction of 4-hydroxybenzaldehyde, acetophenones, malononitrile in the presence of RONA. The synthesized alkoxy arylnicotinonitrile derivatives containing pyridine moiety were predestined as inhibitors for C1018-steel (CS) corrosion in 1.0 M HCl using potentiodynamic-polarization (PDP) and electrochemical impedance spectroscopy (EIS) methods. PDP plots were demonstrated that the arylnicotinonitriles behave as typical inhibitors of the mixed-type. They have also suppressed the CS corrosion at lower [inhibitor] and accomplished an inhibition capacity ranged from 87.6 to 98.2% in 0.7 mM. Their adsorption on the CS interface follows the isotherm model of Langmuir and they include both chemisorption and physisorption mechanisms, with a preference of chemisorption. The morphology of the CS surface was examined utilizing Fourier Transform Infrared Spectroscopy (FTIR) and field-emission scanning electron microscopy (FE-SEM). Moreover, Density Functional Theory (DFT) calculations confirm the empirical findings and the adsorption of arylnicotinonitrile derivatives on the CS interface.

Keywords: Arylnicotinonitrile derivatives; One-pot syntheses; Corrosion inhibition; Surface morphology; DFT calculations; EIS

1. Introduction

Its sufficient mechanistic features, a facility of fabrication and availability and frugal accounts have manufacture carbon steel (CS) the substances of preference in many processing implementations including petroleum refining, production, construction, chemical treatment, and metal treatment equipment [1-4]. Nevertheless, CS has defects of needy corrosion resistance in corrosive acid medium and it might culminate comprehensive harm if utilized without protection. Among the corrosive environments, exceedingly using of hydrochloric acid to eliminate Fe-oxide and rust in industrial treatment including oil-well acidizing, acid-descaling, steel pickling, purifying of boiler pipes, raw treatment, and petroleum processes at temperatures ~ 50-60 °C [5, 6].

One of the generality considerable processes for CS protection from corrosion is applied the inhibitor compounds, which are closely utilized to extenuate metal damage problems in CS immersed in different media. The most widespread corrosion inhibitors are organic molecules related to their beneficial adsorption [7-9]. These organic compounds protect the CS interface *via* the formation of the covering film, which prohibits lineal contact of the CS with the corrosive solution, or it minimizes the corrosion rates, that are produced from either reduction, oxidation and/or both through the prohibiting of the cathodic and/or anodic active centers. The quality of the protection approaches depends fundamentally on the configurations and the inhibitor interaction process with the CS; also it depends on the features of the electrode interface, the corrosive medium, the ionic species and/or the solvent adsorption [10]. The most efficient adsorption of the corrosion inhibitors requires the occurrence of heterocyclic structure containing heteroatoms N, S, O and/or P, double bonds (-C=C-), and lone-pair electrons [11-14]. A vast majority of organic molecules have been suggested as inhibitors for CS corrosion, but many of them are costly and difficult to prepare [15].

Newly, reports strive to the development and design of sustainable compounds for corrosion control [16]. The pyridine moiety has emerged as a substantial scaffold because of its expansion, in diverse natural products and its activity in biological and pharmaceutical chemistry. Pyridine nucleus is also comprised of coordination compounds, surfaces and materials [17]. Among the pyridine construction, alkoxy cyanopyridine compounds have attracted considerable attention due to their broad application [18, 19]. Subsequently, the expansion of new processes for their preparation is still an attractive goal. Newly, the one-pot reaction has earned great interest because of their implementations in chemistry and medicinal, in addition to the synthesis of complex molecules without the isolation of intermediates. Thus, an efficient and safe development for the synthesis of these compounds is still of significance. Hither, the eco-friendly steps for the synthesis of alkoxy arylnicotinonitriles were achieved through one-pot four-component reaction of 4-hydroxybenzaldehyde, acetophenone derivatives, and malononitrile in the presence of sodium alkoxides. In the present work, the four derivatives of 2-alkoxy-4-(4-hydroxyphenyl)-6-arylnicotinonitrile; namely: 4-(4-hydroxyphenyl)-2-methoxy-6-(4-methylphenyl)nicotinonitrile (AHAN-1), sodium 4-[3-cyano-2-(2-ethoxyethoxy)-6-phenylpyridin-4-yl]phenolate (AHAN-2), 2-(2-ethoxyethoxy)-4-(4-hydroxyphenyl)-6-(4-methylphenyl)nicotinonitrile (AHAN-3), and 2-(2-ethoxyethoxy)-4-(4-hydroxyphenyl)-6-(4-methoxyphenyl)nicotinonitrile (AHAN-4) were prepared, studied for corrosion inhibition characteristics and their adsorption on CS in 1.0 M HCl (Scheme 1). The chosen of arylnicotinonitrile derivatives as potent inhibitors for CS corrosion is due to their ease production and the presence of pyridine moiety in their structure with confirming CS protection capabilities. Experimental methods including PDP, EIS, FTIR, and SEM were used to gain knowledge about the adsorption mechanism of the synthesized arylnicotinonitrile at the CS surfaces. Moreover,

DFT calculations were completed on the fabricated inhibitors to reinforce experimental findings.

2. Experimental section

2.1. Instrument, solutions and materials

All information about reagents, reactions, and spectral apparatus: FT-IR, ^1H NMR, ^{13}C NMR and elemental analyses were recorded in **Supporting Information**. The corrosion measurements were performed in the steel (C1018) specimens with the composition: Ni 0.18 %, C 0.19 %, Si 0.15 %, S 0.05 %, Mn 0.73 %, Cr 0.04 %, and balance Fe. Prior each run, the CS specimens were treated mechanically by various SiC emery papers (200, 400, 800, 1200, and 1500), then washed with bidistilled H_2O , and lastly rinsed with acetone. 1.0 M HCl ($\geq 37\%$, pH = 0.3) in the absence and presence of arylnicotinonitrile inhibitors (2×10^{-6} to 7×10^{-4} mol/L) were prepared with bidistilled water.

2.2. Corrosion tests

Electrochemical tests were completed using Gamry Potentiostat/Galvanostat/ZRA workstation (ref-600). Gamry instrument contains EIS300-software for EIS measurements, software DC-105 for Tafel data, and Echem Analyst 6.0 software package for result fitting. The working electrode (WE) is CS. Pt sheet and saturated calomel electrodes (SCE) were utilized as a counter (CE), and reference electrodes (RE), respectively. Before each measurement, the WE (CS) was exposed in the HCl for 50 min to ensure a stationary- status open-circuit potential (E_{OCP}). Experimental procedures of EIS and PDP measurements were similar as described in our previous reports [20, 21].

2.3. General steps for the synthesis of 2-Alkoxy-4-(4-hydroxyphenyl)-6-arylnicotinonitrile (AHAN-1, AHAN-2, AHAN-3, and AHAN-4):

An equimolar amount of 4-hydroxybenzaldehyde (2 mmol, 0.244 g) and

appropriate acetophenones: acetophenone, 4-methyl-, 4-methoxyacetophenone (2 mmol) was added to 4.2 mmol of sodium alkoxide solution (RONa, prepared by dissolving 0.1 g of sodium metal in 50 mL of appropriate alcohol: CH₃OH and/or cellosolve). The reaction mixture was stirred for 30 mins at 25-30 °C and allowed at the same temperature for overnight. Malononitrile (2 mmoles, 0.14 g) was then added to the reaction mixture and refluxed for 2–4 hrs (monitored by TLC). The reaction mixture was allowed to cool and added dropwise onto crushed-ice, (in case AHAN-2, after cooling the reaction, the formed precipitate of AHAN-2 was collected and filtered as sodium salt without acidification). The solution was filtered off from impurities, and the filtrate was acidified by using HCl solution. The formed precipitate was collected, filtered, desiccated and recrystallized from ethyl alcohol.

2.4. Characterization Data of (AHAN-1, AHAN-2, AHAN-3, and AHAN-4):

4-(4-Hydroxyphenyl)-2-methoxy-6-(4-methylphenyl)nicotinonitrile (AHAN-1):

Yield 96 %; white solid; m.p.: 266-267 °C. FTIR (ATR) ν_{\max} 3334 (O-H), 3063, 3019 (C-H aromatic), 2980, 2946 (C-H aliphatic), 2227 (C≡N), 1612 (C=N) cm⁻¹; ¹H NMR δ (ppm): 2.37 (s, 3H, CH₃), 4.10 (s, 3H, OCH₃), 6.94-6.96 (d, J = 8.2 Hz, 2H, CH_{arom.}), 7.30-7.32 (d, J = 7.7 Hz, 2H, CH_{arom.}), 7.58-7.60 (d, J = 8.2 Hz, 2H, CH_{arom.}), 7.62 (s, 1H, CH_{arom.}), 8.08-8.10 (d, J = 7.8 Hz, 2H, CH_{arom.}), 10.05 (s, 1H, OH); ¹³CNMR δ (ppm): 21.4, 54.7, 91.6, 113.3, 116.1, 116.2, 126.8, 127.7, 129.9, 130.6, 134.5, 140.9, 156.6, 157.5, 159.8, 164.9. Elemental Analysis Calcd. (%) for C₂₀H₁₆ O₂N₂ (316.35): N, 8.86; C, 75.93; H, 5.10. Found: N, 8.74; C, 75.88; H, 5.13.

Sodium 4-[3-cyano-2-(2-ethoxyethoxy)-6-phenylpyridin-4-yl]phenolate (AHAN-2):

Yield 95 %; white solid; m.p.: 300-310 °C (Dec.). FTIR (ATR) ν_{\max} 3065 (C-H aromatic), 2974, 2950, 2873 (C-H aliphatic), 2229 (C≡N), 1608 (C=N) cm⁻¹; ¹H NMR δ (ppm): 1.11-1.15 (t, J = 7.0 Hz, 3H, CH₃), 3.53-3.58 (q, J = 7.0 Hz, 2H, CH₃CH₂), 3.80-

3.83 (t, $J = 4.7$ Hz, 2H, CH₂), 4.68-4.70 (t, $J = 4.8$ Hz, 2H, CH₂), 6.95-6.97 (d, $J = 8.6$ Hz, 2H, CH_{arom.}), 7.52-7.55 (m, 3H, CH_{arom.}), 7.62-7.64 (d, $J = 8.6$ Hz, 2H, CH_{arom.}), 7.71 (s, 1H, CH_{arom.}), 8.20-8.22 (m, 2H, CH_{arom.}); ¹³CNMR δ (ppm): 15.5, 66.2, 67.0, 68.3, 92.2, 113.8, 116.1, 116.2, 126.8, 127.8, 129.3, 130.7, 131.0, 137.3, 156.9, 157.5, 159.9, 164.7. Elemental Analysis Calcd. (%) for C₂₂H₁₉N₂NaO₃ (382.38): C, 69.10; H, 5.01; N, 7.33. Found: C, 69.03; H, 4.89; N, 7.31.

2-(2-Ethoxyethoxy)-4-(4-hydroxyphenyl)-6-(4-methylphenyl)nicotinonitrile (AHAN-3):

Yield 94 %; white solid; m.p.: 162-164 °C. IR (ATR) ν_{\max} 3298 (O-H), 3027 (C-H aromatic), 2969, 2917, 2866 (C-H aliphatic), 2229 (C \equiv N), 1615 (C=N) cm⁻¹; ¹H NMR δ (ppm): 1.14-1.15 (t, 3H, CH₃), 2.39 (s, 3H, Ar-CH₃), 3.58 (q, 2H, CH₃CH₂), 3.82 (t, 2H, CH₂CH₂), 4.70 (t, 2H, CH₂CH₂), 6.96 (s, 2H, CH_{arom.}), 7.34 (s, 2H, CH_{arom.}), 7.68 (s, 1H, CH_{arom.}), 8.12 (s, 2H, CH_{arom.}), 9.91 (s, 1H, OH); ¹³CNMR δ (ppm): 15.5, 21.4, 66.2 (disappeared by Dept-135), 66.9 (disappeared by Dept-135), 68.4 (disappeared by Dept-135), 91.8, 113.4, 116.1, 126.9, 127.8, 128.0, 129.9, 130.7, 134.6, 140.9, 156.8, 157.5, 159.8, 164.6. Elemental Analysis Calcd. (%) for C₂₃H₂₂N₂O₃ (374.43): C, 73.78; H, 5.92; N, 7.48. Found: C, 73.72; H, 5.75; N, 7.35.

2-(2-Ethoxyethoxy)-4-(4-hydroxyphenyl)-6-(4-methoxyphenyl)nicotinonitrile (AHAN-4):

Yield 88 %; white solid; m.p.: 200-202 °C. IR (ATR) ν_{\max} 3284 (O-H), 3025 (C-H aromatic), 2974, 2913, 2867 (C-H aliphatic), 2225 (C \equiv N), 1607 (C=N) cm⁻¹; ¹H NMR δ (ppm): 1.13-1.16 (t, $J = 6.9$ Hz, 3H, CH₃), 3.55-3.60 (q, $J = 6.9$ Hz, 2H, CH₃CH₂), 3.81-3.83 (t, $J = 4.3$ Hz, 2H, CH₂), 3.85 (s, 3H, OCH₃), 4.67-4.70 (t, $J = 4.3$ Hz, 2H, CH₂), 6.95-6.97 (d, $J = 8.3$ Hz, 2H, CH_{arom.}), 7.06-7.09 (d, $J = 8.4$ Hz, 2H, CH_{arom.}), 7.61-7.63 (d, $J = 8.3$ Hz, 2H, CH_{arom.}), 7.64 (s, 1H, CH_{arom.}), 8.18-8.20 (d, $J = 8.4$ Hz, 2H, CH_{arom.}), 9.93 (s, 1H, OH); ¹³CNMR δ (ppm): 15.5, 55.9, 66.2 (disappeared by Dept-135), 66.9

(disappeared by Dept-135), 68.4 (disappeared by Dept-135), 91.2, 112.9, 114.8, 116.1, 127.0, 129.5, 129.8, 130.5, 130.6, 156.7, 157.3, 159.8, 161.9, 164.6. Elemental Analysis Calcd. (%) for C₂₃H₂₂O₄N₂ (390.43): H, 5.68; C, 70.75; N, 7.17. Found: H, 5.49; C, 70.82; N, 7.15.

2.5. Surface morphology investigations

The surface morphologies of the CS immersed in the studied corrosive medium free inhibitor and in the presence of 7×10^{-4} mol/L of AHAN-4 for 48 h were determined using a JEOL JSM-6610 LV Scanning Electron Microscope (SEM).

The FTIR spectra of pure AHAN-4 and AHAN-4 adsorbed on the CS interface in 1.0 M hydrochloric acid were performed in 4000–400 cm⁻¹ frequency range. With a view to examine the spectrum of adsorbed AHAN-4 on the CS interface, the sample was exposed in 1.0 M hydrochloric acid containing 7×10^{-4} mol/L of AHAN-4 for 48 h at 323 K. After accomplishment of immersion, the sample was removed, desiccated, and its surface layer was scratched and the consequent powder exposed to FT-IR instrument.

2.6. DFT calculations

Density Functional Theory (DFT) calculations were performed on PC (Pentium III, 733 MHz) using MOPAC2000 [22] with WinMOPAC 2.0 [23] as a graphic interface. Full geometric optimization was accomplished with the semi-empirical PM3 method using the eigenvector-following routine (EF) [24, 25].

3. Results and discussions

3.1. Chemistry

The proposed mechanism for the construction component **5** was presumed to introduce through the formation of chalcones **3** by condensation reaction between acetophenones **1** and 4-hydroxybenzaldehyde **2** in basic medium, (**Scheme 2**). Michael addition of malononitrile **4** on the formed enones **3** gives intermediate **A**. The produced **A**

undergoes a nucleophilic attack by alkoxide anion to yield intermediate **B**, which is easily cyclized to afford the coveted products as previously reported [18]. All AHANs compounds were confirmed by spectral data FTIR, ¹H-, ¹³C-NMR and elemental analyses (*see* Supporting Data).

3.2. PDP measurements

The applied of potentiodynamic-polarization (PDP) tools can be submitted substantial data about the kinetics of corrosion processes [26]. The PDP diagrams of CS in blank 1.0 M hydrochloric acid and containing different concentrations of compound AHAN-4 are presented in Fig. 1(A). PDP plots in the blank (free inhibitors) and inhibited medium containing optimum dose 7×10^{-4} M of all the investigated compounds (AHAN-1, AHAN-2, AHAN-3 and AHAN-4) at 323 K are depicted in Fig. 1 B. It is seen from Fig. 1 (A and B), that both, the anodic CS degradation and cathodic hydrogen development interactions are suppressed after the insertion of AHANs compounds to the corrosive medium. The repressions of the cathodic and anodic reactions are more declared with the raised inhibitor dose and it is lead to increment in inhibition power. The PDP indices, i. e., the cathodic and anodic Tafel slopes (β_c and β_a), the corrosion potential (E_{corr}) and corrosion current density (i_{corr}) are given in Table 1. The i_{corr} was estimated by extrapolation of linear branches of cathodic and anodic plots to the intersection dot. The percentage of inhibition capacity ($\eta_{\text{PDP}}/\%$) and interface coverage (θ) were obtained from the values of i_{corr} by applying the following Eqn. [27] :

$$\eta_{\text{PDP}} / \% = \left(1 - \frac{i_{\text{corr}}^{(i)}}{i_{\text{corr}}^{(0)}} \right) \times 100 = \theta \times 100 \quad (1)$$

where $i_{\text{corr}}^{(i)}$ and $i_{\text{corr}}^{(0)}$ are the inhibited and uninhibited i_{corr} , respectively. As presented in the polarization plot, the cathodic branch shifted to an additional negative potential and the anodic site shifted to a more positive potential. According to the previous studies, if the

shift in E_{corr} is > 85.0 mV, the compound could act as an anodic or cathodic inhibitor, and if its shift is < 85.0 mV, the compound is classified as an inhibitor of the mixed-type [28]. From Table 1, the E_{corr} shift is less than 85 mV for all AHANs compounds, indicating that they are considered as the mixed-type inhibitors.

As observed from Table 1, the values of β_a and β_c are changed by raising the doses of all studied compounds inhibitors, and it elucidates the effect of the inhibitors on the H_2 evolution reaction. The shift in β_c could be attributed to the Cl-/inhibitor species adsorbed onto the metal interface. As presented in Table 1, the values of i_{corr} in the occurrence of AHANs compounds were less than that of the blank corrosive medium at all examined concentrations. Moreover, their i_{corr} values diminished as their doses increment. This means that AHANs compounds would efficiently prohibit CS corrosion. Values of i_{corr} stands at 3.67 mAcm^{-2} in the absence of inhibitors (blank) compared to the AHAN-1 (0.45 mAcm^{-2}), AHAN-2 (0.39 mAcm^{-2}), AHAN-3 (0.24 mAcm^{-2}) and AHAN-4 (0.07 mAcm^{-2}) in the presence of 7×10^{-4} M of inhibitor: $i_{\text{corr}}(\text{blank}) \gg \gg i_{\text{corr}}(\text{AHAN-1}) > i_{\text{corr}}(\text{AHAN-2}) > i_{\text{corr}}(\text{AHAN-3}) > i_{\text{corr}}(\text{AHAN-4})$. The θ values increase with raised in inhibitor concentration. The AHAN inhibitor species are initially adsorbed on the CS interface and covering the available interaction positions. From Table 1, it is reported that the $\eta_{\text{PDP}}/\%$ increase with the increase in [inhibitor] utilized in this investigation. In summary, it is rationalistic to infer that the protection action could be caused by the formulation of the adsorbed layer resulting from the interaction between $-\text{C}\equiv\text{N}-$ and nitrogen hetero-atom and CS interface. Their corrosion inhibition performance follows the sequence of AHAN-4 \gg AHAN-3 $>$ AHAN-2 $>$ AHAN-1.

3.3 EIS studies

More knowledge concerning the features and kinetics of CS corrosion in HCl medium and the inhibition by arylnicotinonitrile compounds was obtained using electrochemical

impedance spectroscopy (EIS). The major characteristics of EIS are to follow the corrosion performance of the CS with time. The Nyquist diagrams of CS in blank 1.0 M HCl and containing varied concentrations of AHAN-4 ($2 \times 10^{-6} \sim 7 \times 10^{-4}$ mol/l) at 50 °C are depicted in Fig. **2A**. The similar plots were recorded for other inhibitors (AHAN-1, AHAN-2 and AHAN-3). Nyquist plot of CS in 1.0 M HCl containing 7×10^{-4} M of different inhibitors at 30 °C is presented in Fig. **2B**. From Fig. **2 A, B**, Nyquist profiles for CS corrosion in uninhibited and inhibited solutions are represented by the imperfect semicircles. These incomplete semicircles increment their diameter with the raised in compound dose, and this imperfection in semicircles is a significance of the adsorption layer formation on the CS interface and a charge transfer approach that controls the CS corrosion in hydrochloric acid solution [29].

Inspection of Nyquist profile in Fig. **2 A, B** displays jointly inductive loops and depressed capacitive at low-frequency (LF) and high-frequency (HF), consecutively. Former investigations have reported that the HF capacitive loop is attributed to the capacitance of double layer (C_{dl}) and charge transfer, while the LF inductive loop is due to the bulk relaxation approach that caused by the adsorption of charged molecules onto the charged CS surfaces [30].

Bode and phase angle modules of CS in 1.0 M hydrochloric acid solution without/with different doses of AHAN-4 at 50 °C are displayed in Fig. **3 A, B**. The phase Bode diagrams (phase angle/ $^{\circ}$ ($|\theta|$) vs. $\log f$) conformable with one semicircle and the Bode impedance profiles ($\log |Z|$ vs. $\log f$) display the impedance of a double layer. This suggests that the corrosion protection kind is monolayer adsorption. The slope values of the linear portion (at intermediate frequencies, $|X|$) of the Bode impedance profile and magnitudes of the maximum phase angle, $|\theta|$ are presented in Table 2. The findings show that $|X|$ is closer to 1 while $|\theta|$ is nearer to 90°, at higher [inhibitor] compared to

the uninhibited system. This indicates that the CS/HCl surface exhibits closer to a perfect capacitor at higher inhibitor concentrations. This also confirms that the inhibitor species adsorbed on the CS interface to form a *pseudo*-capacitive covering layer.

The EIS outcomes were fitted to the equivalent circuit model by ZSimpWin software, and the conformable model is depicted in Fig. 4. In Fig. 4, R_s is the medium resistance, R_p is the resistance of polarization, which comprise the cumulative species at the CS/HCl surface (R_a), the resistance of charge transfer (R_{ct}), the resistance of diffused layer (R_d), and the inhibitor layer resistance at the CS interface (R_i), ($R_p = R_d + R_{ct} + R_i + R_a$) [31]. Constant-phase element (CPE) was utilized in place of the “perfect” double-layer capacitance. The admittance and impedance of the CPE were defined by the next Eqn. [32]:

$$Z_{CPE} = \frac{1}{Y_0} (j\omega)^{-n} \quad \text{and} \quad Y_{CPE} = Y_0 (j\omega)^n \quad (2)$$

where ω represents the angular frequency, Y_0 is the proportionality factor and $j = \sqrt{-1}$ and n is CPE exponent (the deviation indices) is attributed to the rotation angle of pure capacitive streak on the complex-plane diagram, which is mostly near to 1. If $n=0.5$, the CPE is represent for the Warburg impedance; If $n = 1$, the CPE is corresponds to the pure capacitance; and if $n=-1$, the CPE is related to the inductance [31].

The lower n values in the inhibited solution in a comparison with the blank medium indicate that the inhibitor species adsorbed on the CS interface to form a covering layer. Moreover, the n values are close to 1, confirming the *pseudo*-capacitive characteristics of the C-steel/acid interface. The n values are related to the degree of surface heterogeneity. The partially lower n values in the presence of studied compounds compared to the uninhibited medium display that the C-steel interface is relatively more heterogeneous,

which could be due to non-uniform adsorption of the inhibitor molecules on the C-steel substrate.

The EIS parameters including R_s , R_p , CPE, $|\theta|$, $|X|$, n and inhibition capacity ($P_{EIS}/\%$) are tabulated in Table 2. The $P_{EIS}/\%$ values were calculated using Eqn. [32]:

$$P_{EIS}/\% = \left[1 - \frac{R_p^0}{R_p^i} \right] \times 100 \quad (3)$$

where R_p^0 and R_p^i are the R_p in blank and inhibited solutions, respectively. It is observed from Table 2 that the values of R_s were small and nearly comparable to each other.

By examination of the $P_{EIS}/\%$, R_p and CPE values in Table 2, it displays that as [inhibitor] is increased, $P_{EIS}/\%$ and R_p also increases while CPE diminishes. The increasing R_p was supposedly attributed to the formation of a preservative layer on the steel interface, which dramatically prohibited the charge transfer process and dissolution of metal. Furthermore, there was a relatively reduce of the CPE value with the addendum of AHANs compounds. Moreover, the CPE minimized with increasing [AHAN], which is due to the thick covering film [33]. Based on the previous studies [34], the intensity of the adsorbed inhibitor species is raised with diminishing CPE values. Thus, the C_{dl} value result was compatible with the EIS measurements. This is a result of the adsorption of arylnicotinonitrile derivatives on the CS/HCl system which brings about the prohibition of more corrosion of CS.

The increase in $P_{EIS}/\%$ with increasing [inhibitor] might be related to an increment of the number of adsorbed inhibitor species on the metal surface. The order for the protection capacity of the studied arylnicotinonitrile inhibitors within the concentration range considered in this work is AHAN-4 > AHAN-3 > AHAN-2 > AHAN-1. The high protection efficiency for the studied compounds is related to the presence of two benzene rings, N heteroatom, -OH group and lone pairs on O atom, which could be adsorbed on

the CS interface, and progressively formed a dense layer. Although Cl^- ions were collected on the CS surface, this thick layer could separate the Cl^- ions and prohibit the pitting corrosion. The results also indicated that AHAN-4 could efficiently prevent CS corrosion in HCl. This could be related to the molecular structure of AHAN-4 contains a long-chain of $-\text{CH}_2-\text{O}-$, which could cause to form a strong film to protect the CS from corrosion. Furthermore, the highest $P_{\text{EIS}}/\%$ was observed at 7×10^{-4} mol/L, which is in perfect consistency with the findings obtained from the PDP method.

3.4. Surface morphology examinations

3.4.1. FT-IR studies

The Fourier Transform Infrared Spectroscopy (FT-IR) tool is a good method to investigate the adsorption layer producing from the process of adsorption [35]. The FT-IR spectra of the AHAN-4 compound and the adsorption layer formed on the CS in 1.0 M hydrochloric acid containing 7×10^{-4} mol/L of AHAN-4 as an inhibitor are presented in Fig. 5. Arylnicotinonitrile derivatives have various functional groups that possess an electron cloud. This reveals that the adsorption layer between arylnicotinonitrile derivatives and Fe vacant *d*-orbitals is most probably to occur within these functional groups. The FT-IR features for both AHAN-4 and adsorption film were relatively interpreted. The broad peak (peak 1) at about 3284 cm^{-1} corresponds to the $-\text{OH}$ stretching (Fig. 5A). The absence of $-\text{OH}$ band on the inhibited system (adsorbed film) could be related to the chemical bond formation at the CS interface adsorption center (Fig. 5B). Furthermore, the characteristic absorption sharp peaks (Peaks 2 and 3) at 2225 and 1607 cm^{-1} for AHAN-4 compound attributed to $-\text{C}\equiv\text{N}$ and $-\text{CH}=\text{N}-$ bonds, respectively. These peaks for $-\text{C}\equiv\text{N}$ and $-\text{CH}=\text{N}-$ bands in the case of an inhibited system (adsorbed film) were converted to poor absorption peaks at 2179 and 1564 cm^{-1} , respectively. This suggests that electron density of $-\text{C}\equiv\text{N}$ and $-\text{CH}=\text{N}-$ are shifted from $-\text{C}\equiv\text{N}$ and $-\text{CH}=\text{N}-$

groups up to $\text{Fe}^{(II)}$ what causes the formation of Fe-AHAN complex on the CS surface [36]. It was reported that [37], any shift in FT-IR peaks between the inhibitor compounds AHANs and adsorbed film (inhibited system) is attributed to the adsorption of inhibitor compound through ingrained chemical groups. There appears also to interfere with FT-IR vibrational peaks assigned to Fe-O (their source is iron oxide) at 500 and 1400 cm^{-1} that would have been apparent on the FT-IR signatures of the inhibitor adsorbed layer/corrosion product composite (Fig. 5B).

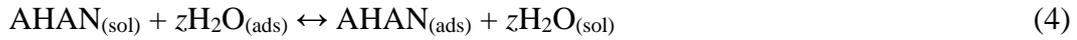
3.4.2. SEM observations

SEM pictures of the pristine CS substrate and after exposed in 1.0 M HCl with/without 7×10^{-4} mol/L of AHAN-4 inhibitor for 48 h at 50 °C are presented in Fig. 6. From Fig. 6A, it is clear that the CS surface before exposure to the corrosive solution exhibits smooth features with immaterial losses that probably attributed to the scratch with different emery papers. Nevertheless, the CS surface immersed in blank 1.0 M hydrochloric acid (free inhibitor) display highly corroded and damaged characteristics because of non-protected exposure to aggressive ions in the corrosive environments (Fig. 6B). The occurrence of AHAN-4 compound as an inhibitor supplied a smoother and cleaner CS surface (Fig. 6C). This demonstrated that the investigated arylnicotinonitrile derivatives adsorb as a preservative layer on the CS surface and block it from a lineal offensive by the corrosive ions in the acidic medium.

3.5. Adsorption isotherms: Thermodynamic parameters

Generally, organic corrosion inhibitors protect metals and alloys *via* adsorbing them onto the surfaces. The adsorption processes may take on a physisorption, chemisorption and/or mixed-type mode. The representative adsorption processes between the steel interface and

inhibitor molecule include the substitution of the adsorbed water molecule at a metal surface based on the following Eqn. [38]:



where AHAN is the arylnicotinonitrile inhibitor and z is the number of water molecules substituted with the adsorbed AHAN species. The capacity of the inhibitor displays the capability to be adsorbed on the steel interface by substituting the H_2O from the metal surface which is attacked by corrosion. Different adsorption models were used to fit the obtained PDP data, such as Flory-Huggins, Langmuir, Freundlich, Frumkin and Temkin isotherms. However, the higher correlation coefficients values (R^2) (Table 3) obtained from the linear relationship indicated that the Langmuir model was the most convenient isotherm. The equation related to the Langmuir isotherm could be qualified as follows [39]:

$$\frac{C_{\text{inhibitor}}}{\theta} = C_{\text{inhibitor}} + \frac{1}{K_{\text{ads}}} \quad (5)$$

where θ is the interface coverage, K_{ads} is the equilibrium adsorption constant and $C_{\text{inhibitor}}$ is [inhibitor]. The linear relationships of $C_{\text{inhibitor}}/\theta$ vs. $C_{\text{inhibitor}}$ are depicted in Fig. 7 for AHAN derivatives. The values of R^2 of the diagrams are near unity (more than 0.999), while the slopes of the plots are more unity, i.e. 1.13 (AHAN-1), 1.11 (AHAN-2), 1.06 (AHAN-3) and 1.01 (AHAN-4). These outcomes confirmed the validity of the Langmuir adsorption model. Moreover, the high K_{ads} values obtained for the investigated AHAN inhibitors reveal that the substitution of H_2O molecules from the metal interface by the inhibitor species, and accordingly the inhibitor adsorption on the CS surface is an adequate process, and the AHAN inhibitors adsorb robustly on the CS interface. From K_{ads} values, the standard free energy of adsorption (ΔG_{ads}^0) can be measured by the following Eqn. [40]:

$$\Delta G_{ads}^0 = -RT \ln(K_{ads} \times 55.50) \quad (6)$$

where $R = 8.314 \text{ J/K mol}$, T is absolute temperature, and the value of 55.5 is the $[\text{H}_2\text{O}]$ in mole L^{-1} . Previous studies indicate that ΔG_{ads}^0 values higher than or around -20.0 kJ/mol are symbolic with physisorption, while values lower than -40.0 kJ/mol is accord with chemical adsorption and values ranged from -20.0 kJ/mol to -40.0 kJ/mol include both physisorption and chemisorption [41]. The negative ΔG_{ads}^0 values (Table 3) indicated that the adsorption process is spontaneous and also confirmed the constancy of the adsorbed layer on the CS surface [42]. It can be inferred from the range of values of ΔG_{ads}^0 in Table 3 that the adsorption mode of AHAN derivatives involves mixed chemisorption and physisorption, with a preference of chemisorption. The trend of the K_{ads} and ΔG_{ads}^0 values is such that $\text{AHAN-4} > \text{AHAN-3} > \text{AHAN-2} > \text{AHAN-1}$ and, which is the same as the relative sequence of the inhibition capacity values.

3.6. DFT calculations

To study the interrelated between the protection capacity of the target molecules (arylnicotinonitrile) and their electronic configuration, DFT calculations were carried out. The study revealed the compatible relationship between the protection capacity ($P\%$) and the calculated quantum chemical indices. The electronic distribution of lowest unoccupied (E_{LUMO}) and highest occupied (E_{HOMO}) molecular orbitals of the investigated models AHAN-1, AHAN-2, AHAN-3 and AHAN-4 are shown in Fig. 8, which reflects that the LUMO and HOMO orbitals are distributed on O, N atoms and phenyl ring. Table 4 displays some thermodynamic values and DFT parameters namely heat of formation (H_f), E_{LUMO} , E_{HOMO} , dipole moment (μ), absolute hardness (η), the energy gap ($\Delta E = E_{LUMO} - E_{HOMO}$), softness (σ) and absolute electronegativity (χ).

E_{HOMO} and E_{LUMO} are important indices for the foretelling of the reactivity of corrosion inhibitor molecules. The donation capability of inhibitor species is often correlating with the E_{HOMO} [43-45]; the high E_{HOMO} values facilitate the absorption power of the inhibitor compound [46]. It is obvious from Table 4, that the values of E_{HOMO} for the target arylnicotinonitrile diminishes in the sequence; AHAN-4 > AHAN-3 > AHAN-2 > AHAN-1, which was found to be compatible with the empirical findings of $P\%$. Also, the calculated values of ΔE were found to be in competing consistently with the $P\%$ with the order: AHAN-4 < AHAN-3 < AHAN-2 < AHAN-1, which is in fully agreed with the order $P\%$ of AHAN-4 > AHAN-3 > AHAN-2 > AHAN-1. Consequently, one can say there is a perfect interrelated between $P\%$ and E_{LUMO} .

A convenient parameter for foretelling of the trend of corrosion processes is dipole moment (μ) which reflects the electron distribution in the molecule as well as its polarity [47]. The absorption of a certain inhibitor increases as the value of its dipole moment (μ) increase and this can be attributed to electronic forces [48]. As shown in Table 4, compound AHAN-4 has the highest μ value compared to other inhibitors which reflect its better inhibition behavior. The values of μ of the investigated arylnicotinonitrile inhibitors are 2.852, 2.479, 2.227 and 2.062 Debye for AHAN-4, AHAN-3, AHAN-2 and AHAN-1, respectively, which is higher than that of H₂O ($\mu = 1.880$ Debye). η is a substantial parameter to gauge the molecular stability and reactivity. A hard compound molecule has a high ΔE and vice versa [49]. In the current report AHAN-4 with low η value, ~ 4.0296 eV compared with the other arylnicotinonitrile inhibitors have a low ΔE and highest $P\%$ [50].

4. Conclusion

In the current report, the corrosion protection action of the fabricated 2-Alkoxy-4-(4-Hydroxyphenyl)-6-arylnicotinonitrile (AHAN) derivatives were studied for CS in 1.0 M hydrochloric acid utilizing empirical and DFT calculations and next conclusions were depicted:

- The 2-Alkoxy-4-(4-Hydroxyphenyl)-6-arylnicotinonitrile (AHAN) derivatives were found to prohibit the CS corrosion in acidic chloride medium and the protection capacity increments with increasing [AHAN].
- The EIS diagrams indicated that the polarization resistance increases and the CPE values were reduced with increasing [AHAN], suggesting that the AHAN species were adsorbed onto the CS surface.
- PDP studies demonstrated that all the synthesized arylnicotinonitrile (AHAN) derivatives are inhibitors of the mixed type.
- Adsorption of the investigated compounds on the CS/HCl interface follows the isotherm of the Langmuir model, with a combined chemisorption and physisorption mechanisms.
- Surface examinations with FE-SEM and FTIR emphasize that the corrosion protection of CS is due to adequate adsorption of AHAN derivatives on the C-steel interface.
- DFT parameters supplied important knowledge to understand the correlation between the inhibition action and molecular structures. The energy gap of these four arylnicotinonitrile inhibitors followed the order AHAN-1 > AHAN-2 > AHAN-3 > AHAN-4, which is consistent with the empirical outcomes.

References

1. M. Goyal, S. Kumar, I. Bahadur, C. Verma, E. E. Ebenso, Organic corrosion inhibitors for industrial cleaning of ferrous and non-ferrous metals in acidic solutions: A review, *J. Mol. Liq.* 256 (2018) 565-573.
2. A. Espinoza-Vázquez, G. E. Negrón-Silva, R. González-Olvera, D. Angeles-Beltrán, H. Herrera-Hernández, M. Romero-Romo, M. Palomar-Pardavé, Mild steel corrosion inhibition in HCl by di-alkyl and di-1, 2, 3-triazole derivatives of uracil and thymine, *Mater. Chem. Phys.* 145 (2014) 407-417.
3. M. Boukalah, A. Ouassini, B. Hammouti, A. E. Idrissi, Corrosion inhibition of steel in sulphuric acid by pyrrolidine derivatives, *Appl. Surf. Sci.* 252 (2006) 2178-2185.
4. P. Morales-Gil, G. Negrón-Silva, M. Romero-Romo, C. Ángeles-Chávez, M. Palomar-Pardavé, Corrosion inhibition of pipeline steel grade API 5L X52 immersed in a 1.0 M H₂SO₄ aqueous solution using heterocyclic organic molecules, *Electrochim. Acta.* 49 (2004) 4733- 4741.
5. A. O. Yüce, G. Kardas, Adsorption and inhibition effect of 2-thiohydantoin on steel corrosion in 0.1 M HCl, *Corros. Sci.* 58 (2012) 86-94.
6. A. P. Hanza, R. Naderi, E. Kowsari, M. Sayebani, Corrosion behavior of mild steel in H₂SO₄ solution with 1, 4-di [1-methylene-3-methyl imidazolium bromide]-benzene as an ionic liquid, *Corros. Sci.*, 107 (2016) 96-106.
7. A. Singh, K.R. Ansari, J. Haque, P. Dohare, H. Lgaz, R. Salghi, M.A. Quraishic, Effect of electron donating functional groups on corrosion inhibition of mild steel in hydrochloric acid: Experimental and quantum chemical study, *J. Taiwan Inst. Chem. Eng.*, 82 (2018) 233-251.

8. A.M. El-Shamy, Kh. Zakaria, M.A. Abbas, S. Zein El Abedin, Anti-bacterial and anti-corrosion effects of the ionic liquid 1-butyl-1-methylpyrrolidinium trifluoromethylsulfonate, *J. Mol. Liq.*, 211 (2015) 363-369.
9. C. Verma, I.B. Obot, I. Bahadur, E.S.M. Sherif, E.E. Ebenso, Choline based ionic liquids as sustainable corrosion inhibitors on mild steel surface in acidic medium: Gravimetric, electrochemical, surface morphology, DFT and Monte Carlo simulation studies, *Appl. Surf. Sci.*, 457 (2018) 134-149.
10. H. M. Abd El-Lateef, M. S. S. Adam, M. M. Khalaf, Synthesis of polar unique 3d metal-imine complexes of salicylidene anthranilate sodium salt. Homogeneous catalytic and corrosion inhibition performance, *J. Taiwan Inst. Chem. Eng.* 88 (2018) 286-304.
11. M. S. S. Adam, H. M. Abd El-Lateef, K.A. Soliman, Anionic oxide-vanadium Schiff base amino acid complexes as potent inhibitors and as effective catalysts for sulfides oxidation: Experimental studies complemented with quantum chemical calculations, *J. Mol. Liq.* 250 (2018) 207-322.
12. H. M. Abd El-Lateef, Synergistic effect of polyethylene glycols and rare earth Ce^{4+} on the corrosion inhibition of carbon steel in sulfuric acid solution: electrochemical, computational, and surface morphology studies, *Res Chem Intermed*, 42 (2016) 3219–3240.
13. M. Palomar-Pardavé, M. Romero-Romo, H. Herrera-Hernández, M.A. Abreu-Quijano, N. V. Likhanova, J. Uruchurtu, J.M. Juárez-García Influence of the alkyl chain length of 2 amino 5 alkyl-1,3,4 thiadiazole compounds on the corrosion inhibition of steel immersed in sulfuric acid solutions, *Corros. Sci.* 54 (2012) 231–243.

14. Y. Qiang, S. Zhang, S. Yan, X. Zou and S. Chen Three indazole derivatives as corrosion inhibitors of copper in a neutral chloride solution, *Corros. Sci.* 126 (2017) 295-304.
15. R. M. Hassan, S. M. Ibrahim, H. D. Takagi, S. A. Sayed. Kinetics of corrosion inhibition of aluminum in acidic media by water-soluble natural polymeric chondroitin-4- sulfate as anionic polyelectrolyte inhibitor, *Carbohydr. Polym.* 192 (2018) 356-363.
16. E. Saei, B. Ramezanzadeh, R. Amini, and M. S. Kalajahi, Effects of combined organic and inorganic corrosion inhibitors on the nanostructure cerium based conversion coating performance on AZ31 magnesium alloy: Morphological and corrosion studies, *Corros. Sci.* 125 (2017) 186-200.
17. D. Khalili, Graphene oxide: a reusable and metal-free carbocatalyst for the one-pot synthesis of 2-amino-3-cyanopyridines in water, *Tetrahedron Letters* **57** (2016) 1721–1723.
18. A. A. Amer, AA Abdelhamid, Microwave-Assisted, One-Pot Multicomponent Synthesis of Some New Cyanopyridines, *J. Heterocycl. Chem.* 54 (6) (2017) 3126-3132.
19. K.A.M. Abouzid, G. H. Al-Ansary, A.M. El-Naggar, Eco-friendly synthesis of novel cyanopyridine derivatives and their anticancer and PIM-1 kinase inhibitory activities, *European Journal of Medicinal Chemistry*, 134 (2017) 357-365,.
20. M.M. Saleh, Manal G. Mahmoud, Hany M. Abd El-Lateef, Comparative study of synergistic inhibition of mild steel and pure iron by 1-hexadecylpyridinium chloride and bromide ions, *Corro.Sci.*154 (2019) 70–79.

21. H. M. Abd El-Lateef, Experimental and Computational Investigation on the Corrosion Inhibition Characteristics of mild steel by some novel synthesized imines in Hydrochloric acid Solutions, *Corros. Sci.* 92 (2015) 104–117.
22. J. J. P. Stewart, *Mopac2000 Manual*, Fujitsu Limited, Tokyo, Japan, 1999.
23. Win Mopac 2.0, *User Manual*, Fujitsu Limited, Tokyo, Japan (1997-98).
24. J. Baker, An Algorithm for the Location of Transition States, *J. Comp. Chem.*; 7 (1986) 385-395.
25. J. J. P. Stewart, Optimization of parameters for semiempirical methods. II Extension of PM3 to Be, Mg, Zn, Ga, Ge, As, Se, Cd, In, Sn: Sb, Te, Hg, Tl, Pb, and Bi, *J. Comp. Chem.*, 12 (1991) 320-341.
26. B. Xu, Y. Ji, X. Zhang, . X. Jin, W. Yang, Y. Chen, Experimental and theoretical studies on the corrosion inhibition performance of 4-amino-N,N- di-(2-pyridylmethyl)-aniline on mild steel in hydrochloric acid, *RSC Adv.*, 5 (2015) 56049-56059.
27. X. Wang, H. Yang, F. Wang, Inhibition performance of a gemini surfactant and its co-adsorption effect with halides on mild steel in 0.25 M H₂SO₄ solution, *Corro. Sci.* 55 (2012) 145–152.
28. E. S. Ferreira, C. Giancomelli, F. C. Giacomelli, A. Spinelli, Evaluation of the inhibitor effect of L-ascorbic acid on the corrosion of mild steel, *Mater. Chem. Phys.*, 83 (2004) 129-134.
29. L. C. Murulana, M. M. Kabanda, E.E. Ebenso, Experimental and theoretical studies on the corrosion inhibition of mild steel by some sulphonamides in aqueous HCl, *RSC Adv.*, 5 (2015) 28743 –28761
30. K. S. Jacob and G. Parameswaran, Corrosion inhibition of mild steel in hydrochloric acid solution by Schiff base furoin thiosemicarbazone, *Corros. Sci.*, 52 (2010) 224–228.

31. H. H. Hassan, E. Abdelghani and M. A. Amin, Inhibition of mild steel corrosion in hydrochloric acid solution by triazole derivatives: Part I. Polarization and EIS studies, *Electrochim. Acta*, 52 (2007) 6359–6366.
32. A. Y. Musa, A. A. H. Kadhum, A. B. Mohamad and M. S. Takri, Experimental and theoretical study on the inhibition performance of triazole compounds for mild steel corrosion, *Corros. Sci.*, 52 (2010) 3331-3340.
33. M. A. Hegazy, M. Abdallah, H. Ahmed, Novel cationic gemini surfactants as corrosion inhibitors for carbon steel pipelines, *Corro. Sci.* 52 (2010) 2897–2904.
34. M. A. Hegazy, A.S. El-Tabei, A.H. Bedair, M.A. Sadeq, Synthesis and inhibitive performance of novel cationic and gemini surfactants on carbon steel corrosion in 0.5 M H₂SO₄ solution, *RSC Adv.*, 5 (2015) 64633-64650.
35. K. B. Benzoni, H. Tresa Varghese, C. Y. Panicker, K. Pradhan, B. K. Tiwary, A. K. Nanda and C. V. Alsenoy, Spectrochim. Spectroscopic investigation (FT-IR and FT-Raman), vibrational assignments, HOMO–LUMO, NBO, MEP analysis and molecular docking study of 2-(4-hydroxyphenyl)-4,5-dimethyl-1H-imidazole 3-oxide, *Acta, Part A*, 146 (2015) 307–322.
36. T. Polat, S. Yurdakul, Quantum chemical and spectroscopic (FT-IR and FT-Raman) investigations of 3-methyl-3h-imidazole-4-carbaldehyde, *Spectrochim. Acta, Part A*, 133 (2014) 683–696.
37. B. Morzyk-Ociepa, E. Rózycka-Sokołowska and D. Michalska, Revised crystal and molecular structure, FT-IR spectra and DFT studies of chlorotetrakis(imidazole)copper(II) chloride, *J. Mol. Struct.*, 1028 (2012) 49 –56.
38. M. M. Solomon, S.A. Umoren, I.I. Udosoro, A.P. Udoh, Inhibitive and adsorption behavior of carboxymethyl cellulose on mild steel corrosion in sulphuric acid solution, *Corros. Sci.* 52 (2010) 1317–1325.

39. M. T. Alhaffar, S.A. Umoren, I.B. Obot, S.A. Ali, Isoxazolidine derivatives as corrosion inhibitors for low carbon steel in HCl solution: experimental, theoretical and effect of KI studies, *RSC Adv.* 8 (2018) 1764–1777.
40. A. A. Atia, M.M. Saleh, Inhibition of acid corrosion of steel using cetylpyridinium chloride, *J. Appl. Electrochem.* 33 (2003) 171–177.
41. P. Roy, A. Pal, D. Sukul, Origin of the synergistic effect between polysaccharide and thiourea towards adsorption and corrosion inhibition for mild steel in sulphuric acid, *RSC Adv.* 4 (2014) 10607–10613.
42. H. M. Abd El-Lateef, Corrosion inhibition characteristics of a novel salicylidene isatin hydrazine sodium sulfonate on carbon steel in HCl and a synergistic nickel ions additive: A combined experimental and theoretical perspective, *Appl. Surf. Sci.* 501 (2020) 144237
43. N.O. Eddy, E.E. Ebenso, Quantum chemical studies on the inhibition potentials of some penicillin compounds for the corrosion of mild steel in 0.1 M HCl, *J. Mol. Model* 16 (7) (2010) 1291-1306.
44. E.E. Ebenso, T. Arslan, F. Kandemirli, N. Caner, I. Love, Quantum chemical studies of some rhodanine azosulpha drugs as corrosion inhibitors for mild steel in acidic medium, *Int. J. Quantum Chem.* 110 (2010) 1003-1018.
45. S. Xia, M. Qiu, L. Yu, F. Liu, H. Zhao, Molecular dynamics and density functional theory study on relationship between structure of imidazoline derivatives and inhibition performance, *Corros. Sci.* 50 (2008) 2021-2029.
46. T. Arslan, F. Kandemirli, E.E. Ebenso, I. Love, H. Alemu, Quantum chemical studies on the corrosion inhibition of some sulphonamides on mild steel in acidic medium, *Corros. Sci.* 51 (2009) 35-47.

47. L. Herrag, B. Hammouti, S. Elkadiri, A. Aouniti, C. Jama, H. Vezin, F. Bentiss, Adsorption properties and inhibition of mild steel corrosion in hydrochloric solution by some newly synthesized diamine derivatives: experimental and theoretical investigations, *Corros. Sci.* 52 (2010) 3042-3051.
48. M. Lashkari, M.R. Arshadi, DFT studies of pyridine corrosion inhibitors in electrical double layer: solvent, substrate, and electric field effects, *Chem. Phys.* 299 (2004) 131-137.
49. N.O. Obi-Egbedi, I.B. Obot, M.I. El-Khaiary, S.A. Umoren, E.E. Ebenso, Computational simulation and statistical analysis on the relationship between corrosion inhibition efficiency and molecular structure of some phenanthroline derivatives on mild steel surface, *Int. J. Electro Chem. Sci.* 6 (2011) 5649-5675.
50. H. M. Abd El-Lateef, A. M. Abu-Dief, M. A.A. Mohamed, Corrosion inhibition of carbon steel pipelines by some novel Schiff base compounds during acidizing treatment of oil wells studied by electrochemical and quantum chemical methods, *J. Mol. Struct.*, 1130 (2017) 522-542.

List of Tables

No.	Caption
TABLE 1	PDP parameters and inhibition capacity for CS in 1.0 M HCl in the absence and presence of various concentrations of arylnicotinonitrile inhibitors at 50 °C
TABLE 2	EIS parameters and inhibition capacity for CS in 1.0 M HCl in the absence and presence of various concentrations of arylnicotinonitrile inhibitors at 50 °C
TABLE 3	Adsorption parameters for CS in 1.0 M hydrochloric acid for the applied inhibitors at 50 °C using PDP (estimated from the Langmuir adsorption model)
TABLE 4	DFT parameters for the synthesized arylnicotinonitrile derivatives

Table 1:

Inhibitors code	C_{inh}/M	$I_{corr} \pm SD/ mAcm^{-2}$	$-E_{corr}/ mV (SCE)$	$\beta_a/ mV dec^{-1}$	$-\beta_c/ mV dec^{-1}$	θ	$PPDP/\%$
Blank	0.0	3.67±0.37	461	115	208	-	-
AHAN-1	2×10^{-6}	2.29±0.25	464	129	225	0.375	37.5
	7×10^{-6}	1.89±0.20	467	129	240	0.484	48.4
	2×10^{-5}	1.43±0.13	474	126	244	0.608	60.8
	7×10^{-5}	1.12±0.11	454	127	216	0.693	69.3
	2×10^{-4}	0.77±0.09	463	130	224	0.789	78.9
	7×10^{-4}	0.45±0.03	475	133	235	0.876	87.6
AHAN-2	2×10^{-6}	2.23±0.22	460	130	243	0.392	39.2
	7×10^{-6}	1.75±0.16	465	134	236	0.523	52.3
	2×10^{-5}	1.31±0.12	463	129	228	0.641	64.1
	7×10^{-5}	0.96±0.10	458	132	229	0.736	73.6
	2×10^{-4}	0.64±0.07	455	137	222	0.824	82.4
	7×10^{-4}	0.39±0.02	467	139	235	0.893	89.3
AHAN-3	2×10^{-6}	1.98±0.16	463	127	244	0.459	45.9
	7×10^{-6}	1.60±0.14	468	130	224	0.563	56.3
	2×10^{-5}	1.16±0.12	469	129	236	0.683	68.3
	7×10^{-5}	0.84±0.08	459	127	237	0.771	77.1
	2×10^{-4}	0.51±0.04	454	135	238	0.862	86.2
	7×10^{-4}	0.24±0.02	471	131	243	0.934	93.4
AHAN-4	2×10^{-6}	1.84±0.18	467	127	238	0.498	49.8
	7×10^{-6}	1.45±0.15	463	133	242	0.604	60.4
	2×10^{-5}	0.93±0.10	461	132	243	0.746	74.6
	7×10^{-5}	0.56±0.06	459	125	235	0.846	84.6
	2×10^{-4}	0.30±0.03	480	129	234	0.919	91.9
	7×10^{-4}	0.07±0.01	483	131	236	0.982	98.2

Table 2:

Inhibitors code	$C_{inh}/$ mol L⁻¹	$R_s/$ Ω cm²	$CPE/$ μF cm⁻²	$R_p/$ Ω cm²	n	$ \theta /^\circ$	$ X $	$P_{EIS}/\%$
Blank	0.0	0.26	285.4	17.2±1.3	0.891	36.3	0.765	-
AHAN-1	2×10 ⁻⁶	0.33	197.5	22.5±1.6	0.814	38.6	0.874	23.5
	7×10 ⁻⁶	0.53	171.2	35.3±2.7	0.832	40.1	0.756	51.2
	2×10 ⁻⁵	0.79	120.7	76.4±6.5	0.823	45.5	0.811	77.4
	7×10 ⁻⁵	1.20	91.1	97.3±8.1	0.843	54.7	0.798	82.3
	2×10 ⁻⁴	1.65	69.8	144.7±12.3	0.837	62.4	0.845	88.1
	7×10 ⁻⁴	2.02	43.7	196.1±15.8	0.841	80.1	0.789	91.2
AHAN-2	2×10 ⁻⁶	0.30	171.7	25.7±2.2	0.830	39.7	0.861	33.1
	7×10 ⁻⁶	0.48	148.8	43.8±3.7	0.848	41.4	0.831	60.7
	2×10 ⁻⁵	0.72	104.9	93.1±8.4	0.839	48.1	0.892	81.5
	7×10 ⁻⁵	1.08	79.2	123.6±10.8	0.859	57.5	0.877	86.1
	2×10 ⁻⁴	1.49	60.6	176.4±16.1	0.853	65.8	0.929	90.2
	7×10 ⁻⁴	1.83	38.3	215.5±20.5	0.857	82.3	0.867	92.0
AHAN-3	2×10 ⁻⁶	0.29	143.1	32.6±2.7	0.838	43.7	0.832	47.2
	7×10 ⁻⁶	0.5	124.4	53.8±4.2	0.856	43.1	0.721	68.1
	2×10 ⁻⁵	0.77	87.4	116.4±9.8	0.847	50.6	0.772	85.2
	7×10 ⁻⁵	1.19	66.8	168.5±14.4	0.868	60.6	0.767	89.8
	2×10 ⁻⁴	1.66	50.5	221.3±19.8	0.862	69.3	0.804	92.2
	7×10 ⁻⁴	2.05	31.9	255.9±22.2	0.866	84.2	0.751	93.2
AHAN-4	2×10 ⁻⁶	0.35	106.7	39.3±3.1	0.854	45.7	0.817	56.2
	7×10 ⁻⁶	0.56	92.1	64.7±5.6	0.873	49.3	0.793	73.4
	2×10 ⁻⁵	0.83	64.7	132.8±11.1	0.864	55.2	0.851	87.1
	7×10 ⁻⁵	1.25	49.4	192.5±16.6	0.885	64.9	0.838	91.1
	2×10 ⁻⁴	1.72	37.4	279.6±23.7	0.878	71.2	0.887	93.8
	7×10 ⁻⁴	2.11	23.6	325.9±29.5	0.883	87.5	0.828	94.7

Table 3:

Inhibitor	R^2	S=slope	$K_{ads} (M^{-1})$	$\Delta G_{ads}^0 / kJ mol^{-1}$
AHAN-1	0.9995	1.13	7.77×10^4	-39.75
AHAN-2	0.9997	1.11	9.61×10^4	-40.32
AHAN-3	0.9997	1.06	10.42×10^4	-40.51
AHAN-4	0.9998	1.01	13.21×10^4	-41.13

Table 4:

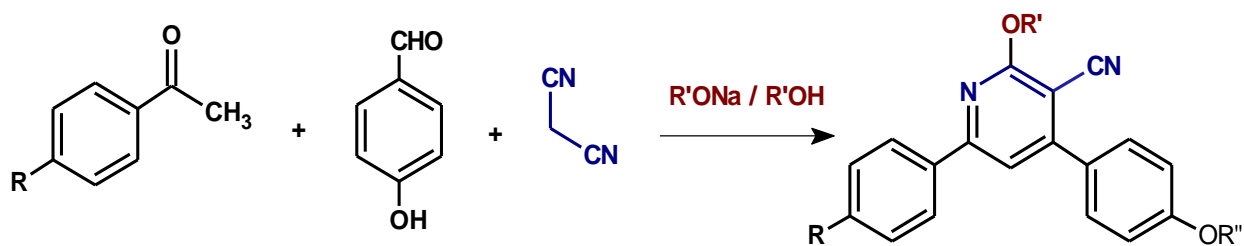
Comp. No.	ΔH (kcal/mol)	Dipole moment (μ, debye)	E_{HOMO} (eV)	E_{LUMO} (eV)	ΔE ($E_{\text{HOMO}} - E_{\text{LUMO}}$)	(χ)	(η)	(σ)
AHAN-1	-13.0024	2.062	-9.1947	-0.9204	8.2743	5.0575	4.1371	0.2417
AHAN-2	30.6443	2.227	-9.1247	-0.9040	8.2207	5.0143	4.1103	0.2432
AHAN-3	-21.1124	2.470	-9.0880	-0.8727	8.2153	4.9803	4.1076	0.2434
AHAN-4	-51.6260	2.852	-8.9169	-0.8577	8.0592	4.8873	4.0296	0.2481

(χ) = Absolute Electronegativity, (η) = Global Hardness, (σ) = Softness

LIST OF FIGURES

No.	Caption
Scheme 1	Schematic representation for the synthetic procedure of arylnicotinonitrile compounds (AHAN-1, AHAN-2, AHAN-3, and AHAN-4)
Scheme 2	The postulated reaction mechanism for the synthesis of 2-alkoxy-4-(4-hydroxyphenyl)-6-arylnicotinonitriles 5.
Figure 1	PDP curves of CS in 1.0 M HCl solution without and with various concentrations of (A) AHAN-4 and (B) containing 7×10^{-4} M of different inhibitors at 50 °C.
Figure 2	Nyquist plots of CS in 1.0 M HCl solution without and with various concentrations of (A) RN-4 and (B) containing 7×10^{-4} M of different inhibitors at 50 °C.
Figure 3	Bode (A) and phase angle (B) plots of CS in 1.0 M HCl solution without and with various concentrations of AHAN-4 at 50 °C.
Figure 4	Equivalent circuit used to fit the EIS data obtained for CS corrosion in 1.0 M HCl in the absence and presence of arylnicotinonitrile compounds
Figure 5	FTIR spectra of (A) crude AHAN-4 compound and (b) adsorption layer formed on the CS in 1.0 M HCl in the presence of 7×10^{-4} mol/l of AHAN-4 inhibitor.
Figure 6	SEM images of (A) pristine CS, (B) CS immersed in 1.0 M HCl for 48 h and (C) CS immersed in 1.0 M HCl containing 7×10^{-4} mol/l of AHAN-4 inhibitor for 48 h.
Figure 7	Langmuir adsorption model for the corrosion of CS in 1.0 M hydrochloric acid containing the investigated inhibitors at 50 °C: (A) AHAN-1, (B) AHAN-2, (C) AHAN-3 and (D) AHAN-4 (from PDP method).
Figure 8	Molecular orbital surface and HOMO-LUMO energy gap for HOMO and LUMO of some cyanopyridine derivatives obtained by PM3 semi-empirical method

Scheme 1



AHAN-1; $R = CH_3, R' = CH_3, R'' = H$

AHAN-2; $R = H, R' = CH_2CH_2OCH_2CH_3, R'' = Na$

AHAN-3; $R = CH_3, R' = CH_2CH_2OCH_2CH_3, R'' = H$

AHAN-4; $R = OCH_3, R' = CH_2CH_2OCH_2CH_3, R'' = H$

Scheme 2

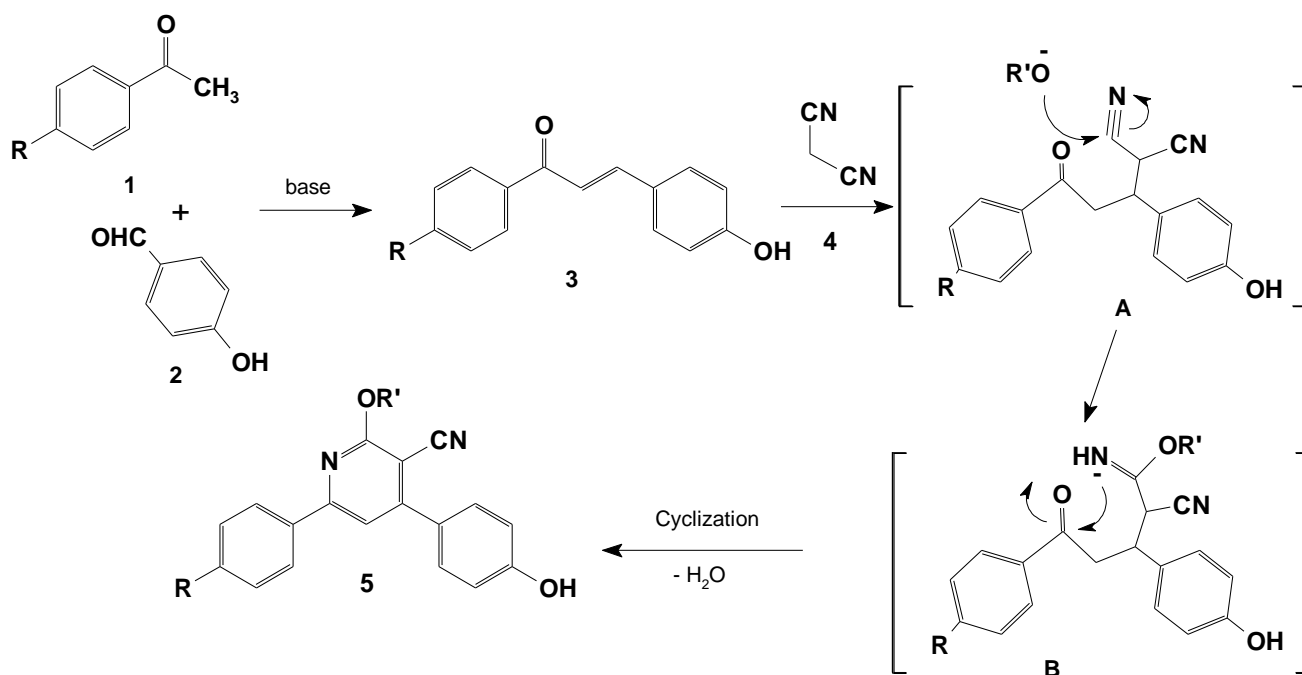


Figure 1

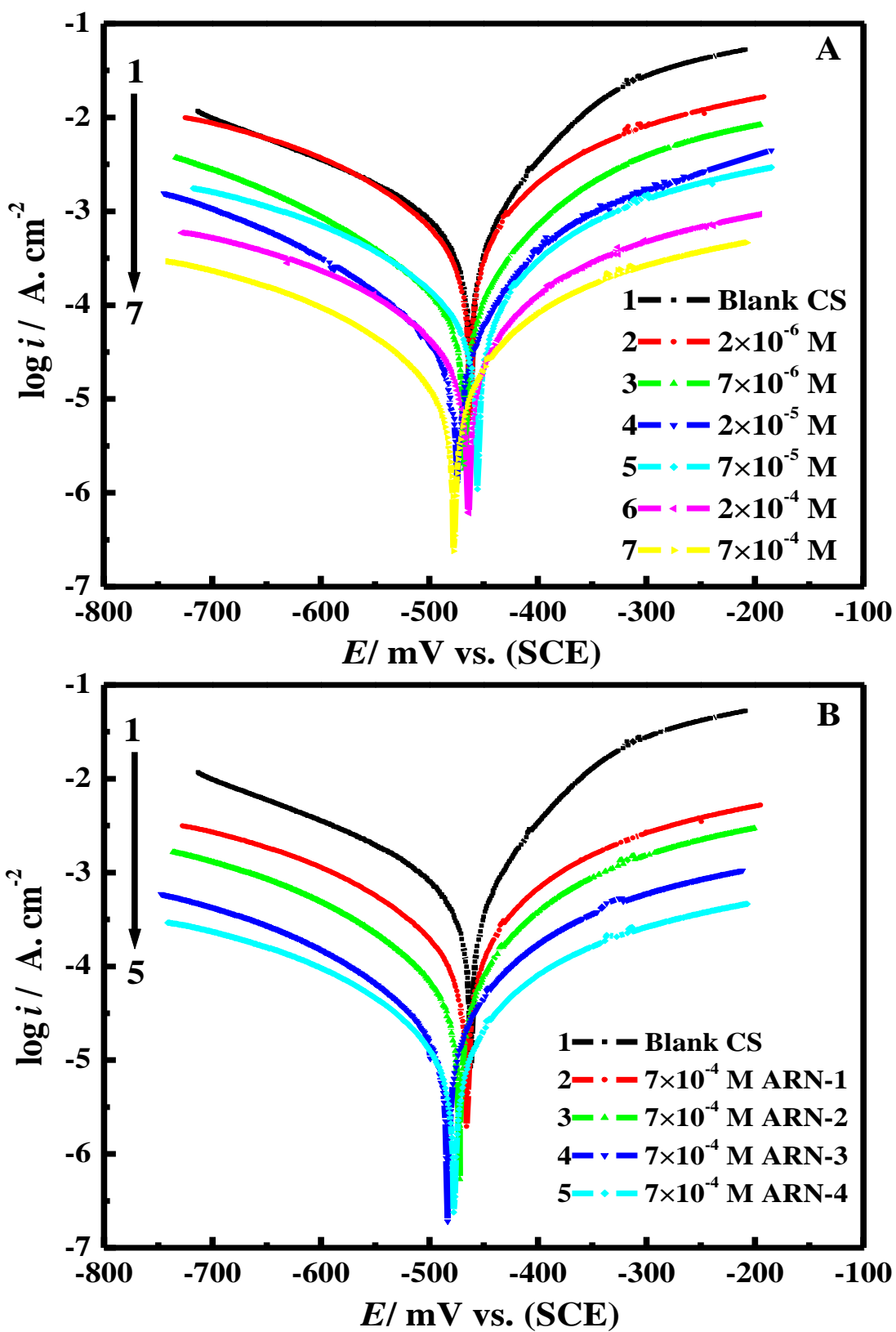


Figure 2

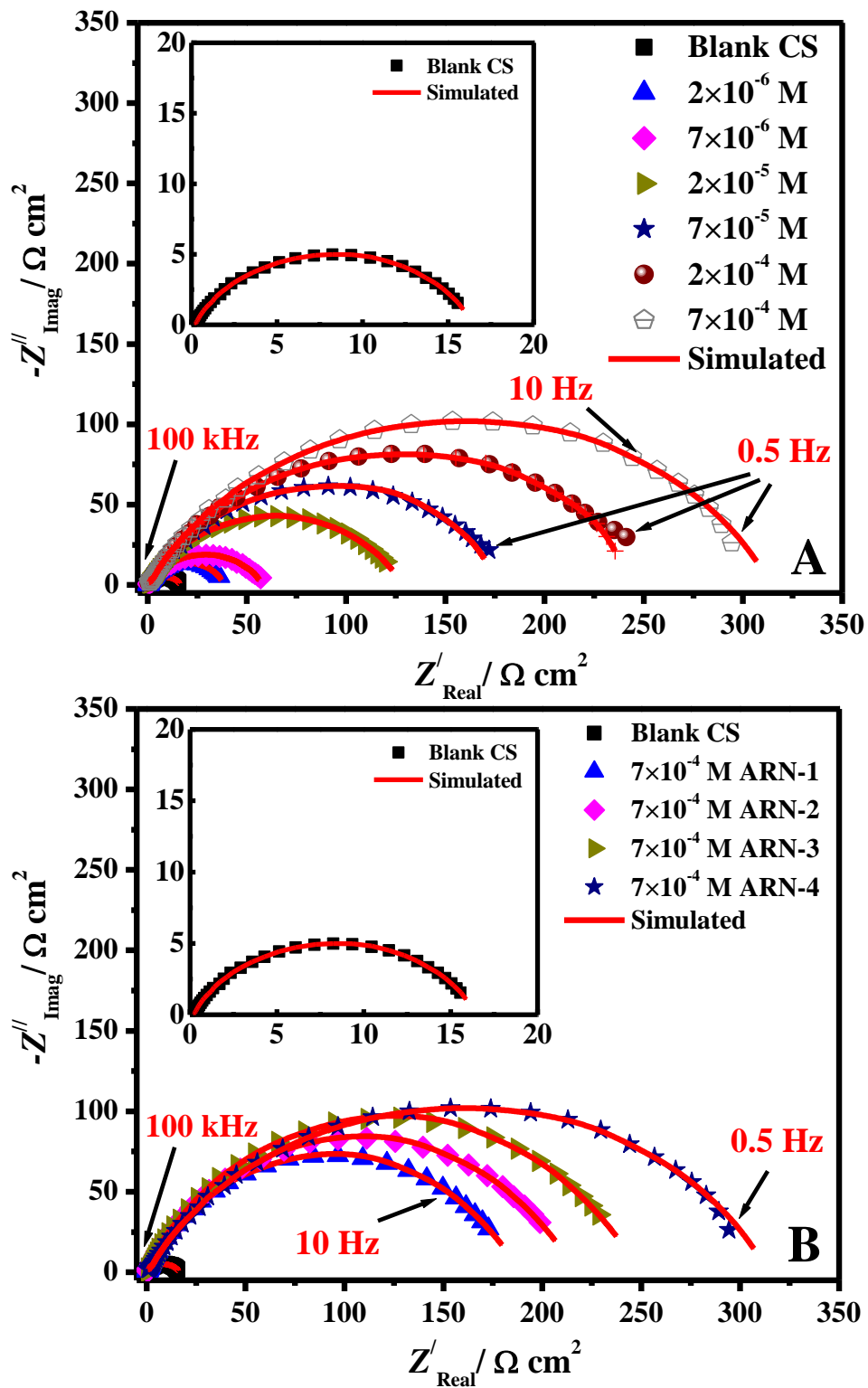


Figure 3

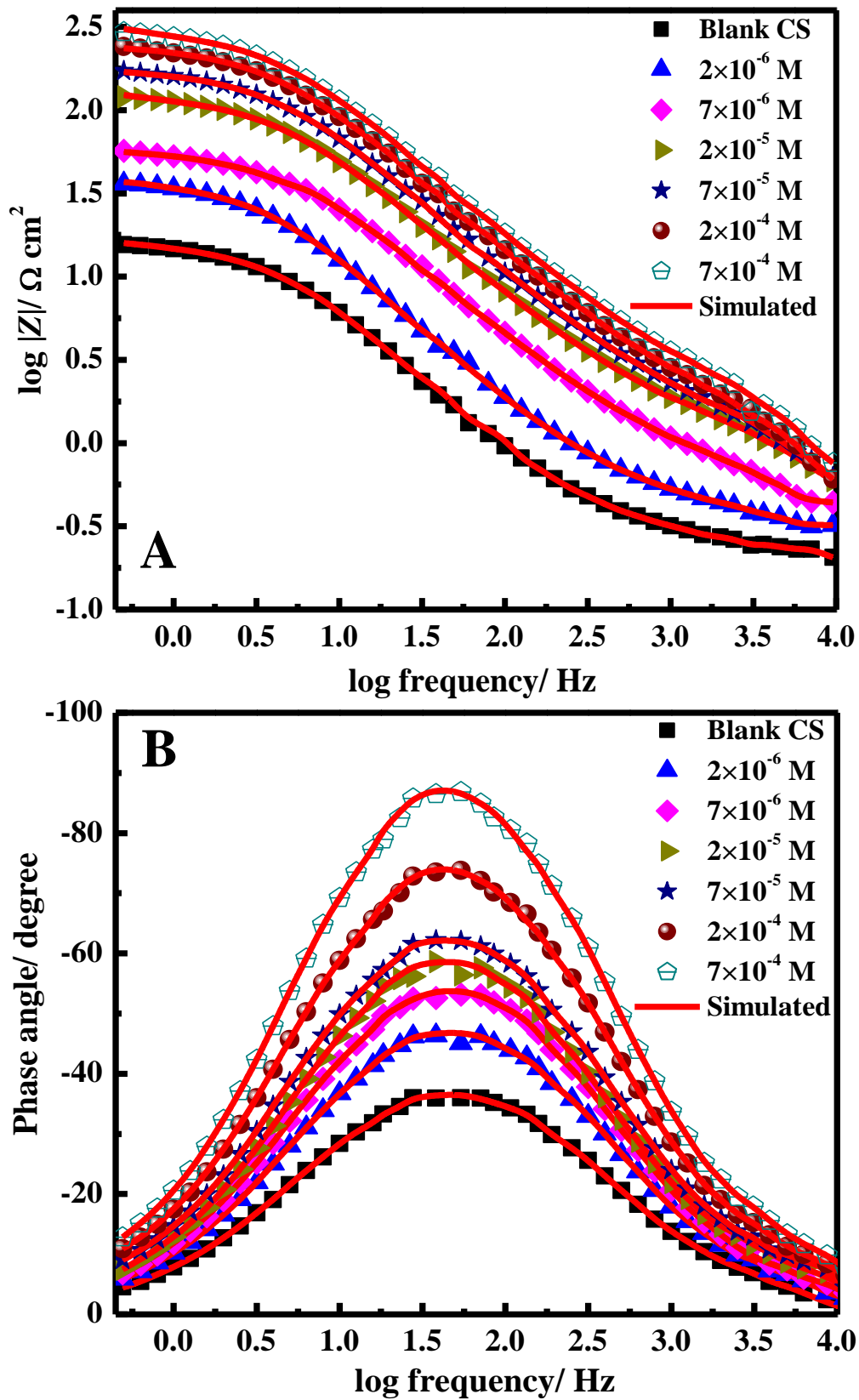


Figure 4

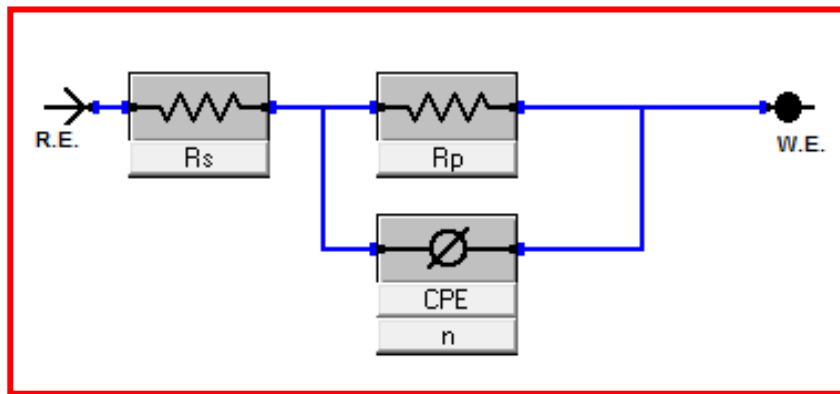


Figure 5

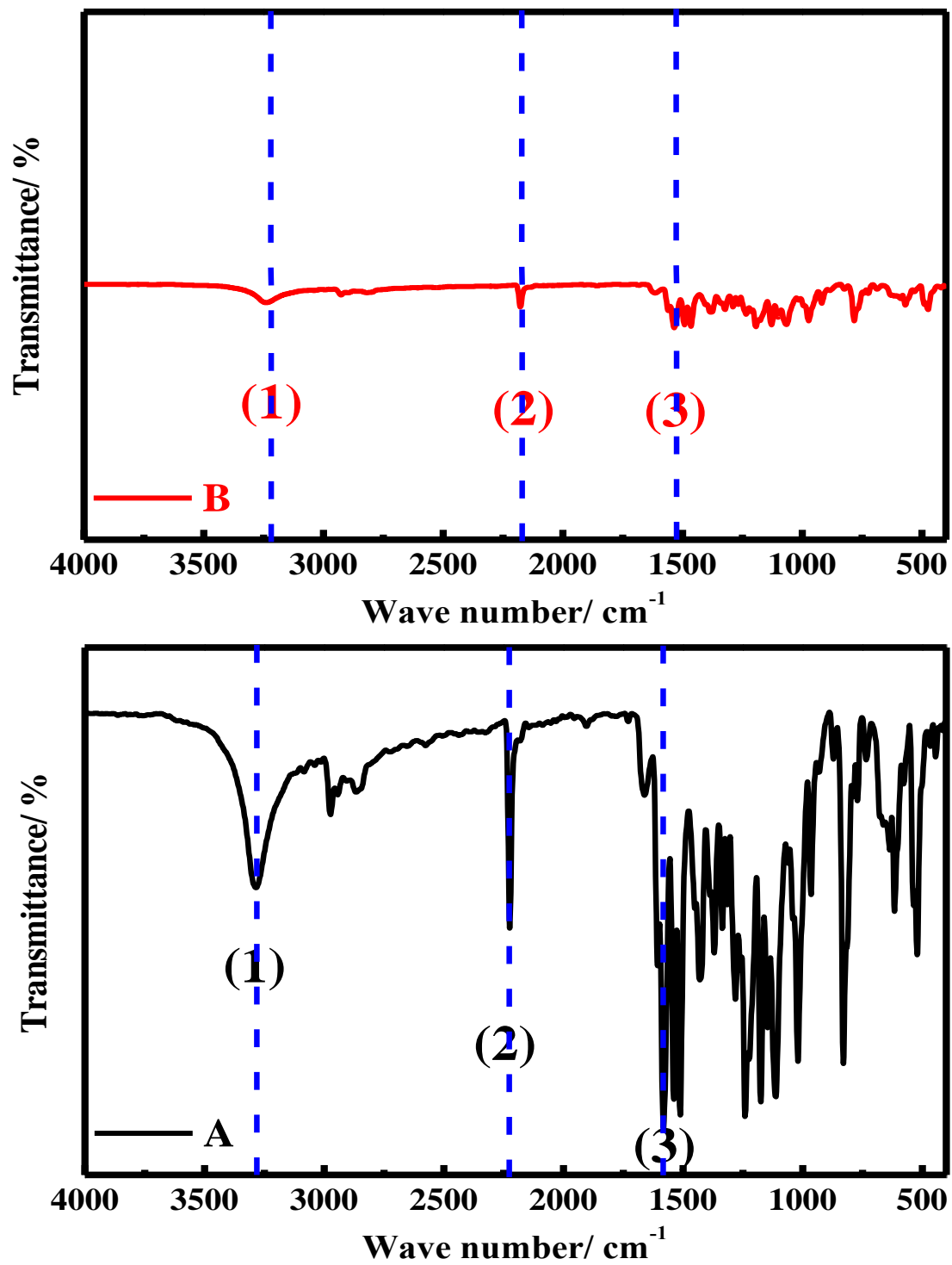


Figure 6

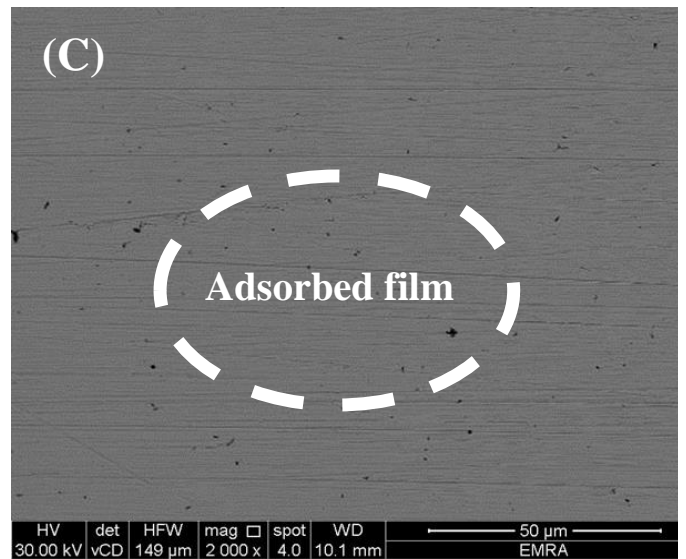
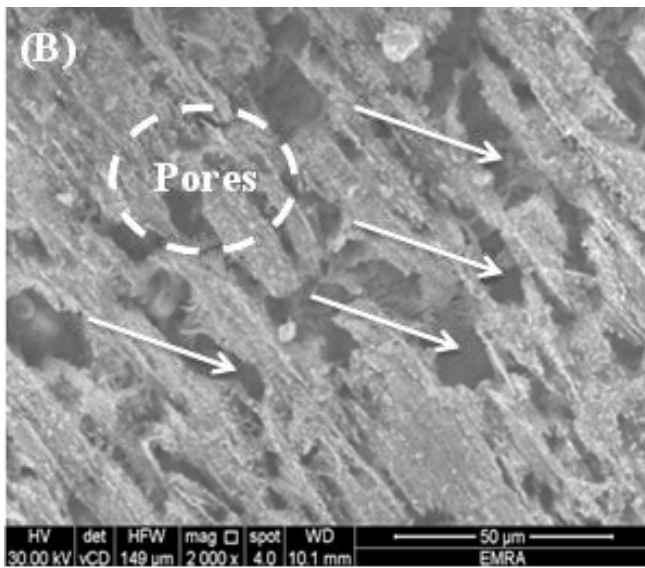
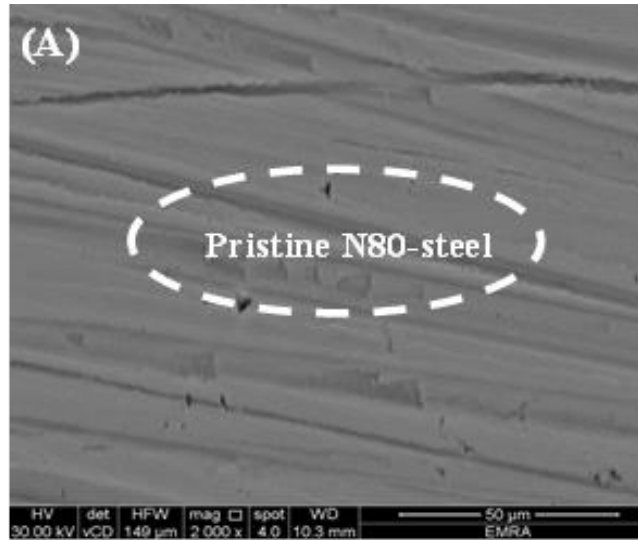


Figure 7

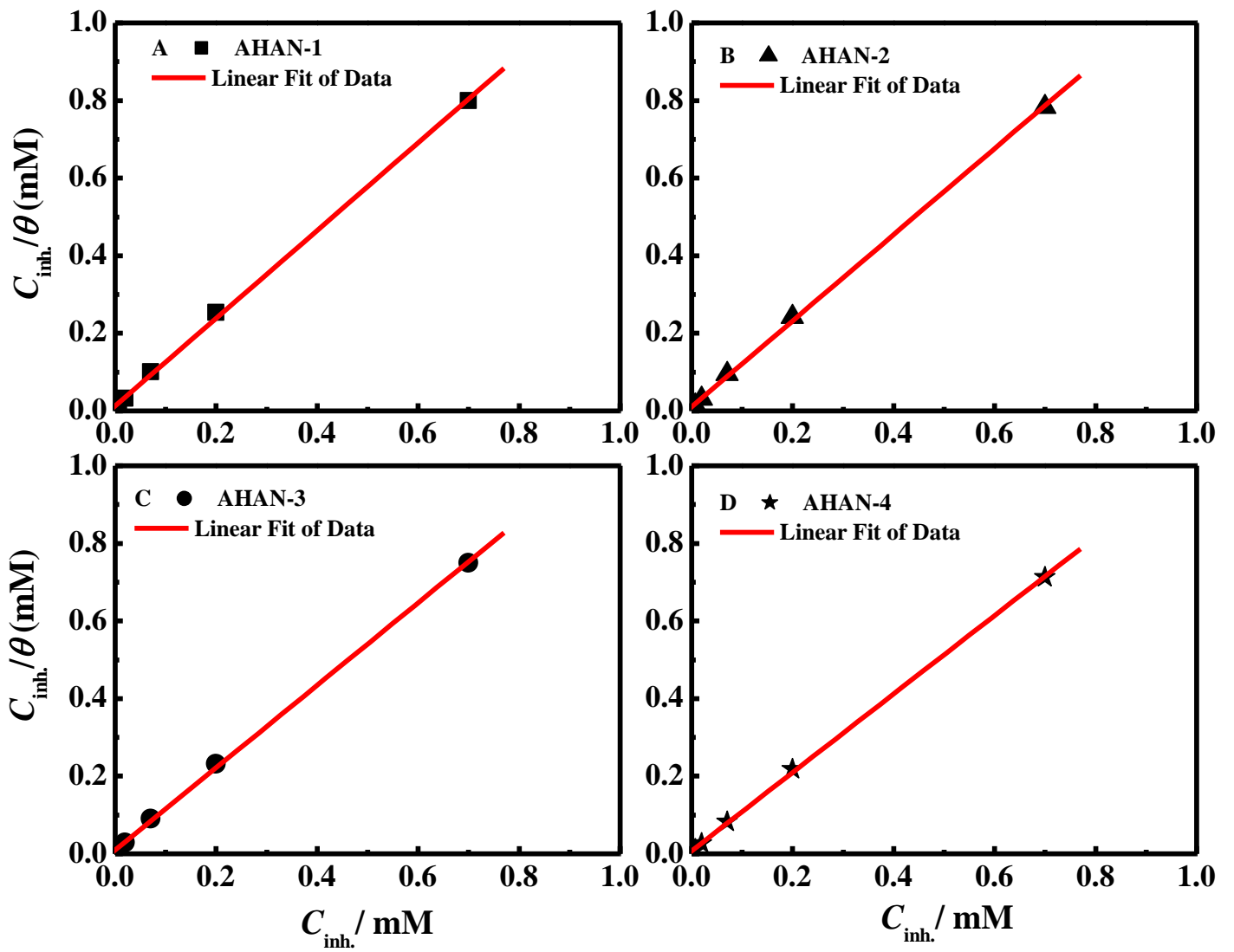


Figure 8

